ELSEVIER

Chemical Engineering Science 60 (2005) 5499–5512

Chemical Engineering Science

www.elsevier.com/locate/ces

Viscous liquid sheets and operability bounds in extrusion coating

Steven J. Weinstein*, Alain Gros

Eastman Kodak Company, Rochester, NY 14652-3703, USA

Received 7 February 2005; received in revised form 6 April 2005; accepted 15 April 2005
Available online 1 July 2005

Abstract

The steady-state extrusion coating of an extremely viscous power-law liquid from a slot and onto a moving substrate across a narrow gap is examined. A key feature of this configuration is a two-dimensional liquid sheet that bridges the gap and might be subjected to an ambient pressure drop across its wide faces. The local thickness of this sheet may be viewed as gradually thinning from the slot to the substrate, and simplified equations governing its shape are derived. Analytical solutions for the shape of the liquid sheet, and the flow within, are obtained in the limit where viscous and pressure forces dominate all others. It is found that the centerline shape of the liquid sheet is circular when a pressure drop is applied, despite the fact that surface tension forces, which typically give rise to circular shapes in narrow gaps, are neglected. Nevertheless, it is analytically shown that the stretching of the viscous-dominated liquid sheet gives rise to an effective tension that plays an analogous role to surface tension. The range of possible applied pressures is thus deduced via geometrical considerations of a circular shape constrained in the narrow gap, as in the analogous surface-tension-dominated analysis (Ruschak, 1976. Chemical Engineering Science 31, 1057); extrusion coating fails when a liquid sheet cannot be constructed successfully.

Keywords: Fluid mechanics; Modeling; Non-Newtonian fluids; Films; Coating; Liquid sheet

1. Introduction

Liquid films of high uniformity are deposited onto moving substrates in coating processes used to manufacture photographic films, inkjet papers, and plastic sheets. The most sophisticated coating methods involve a die distributor that is used to create wide and thin liquid sheets in preparation for coating. As the flow rate to the die and substrate speed are specified, a desired coated film thickness may be specified, regardless of variations in fluid properties. Such methods are referred to as "pre-metered," to distinguish them from "self-metered" methods in which fluid properties greatly affect coated thickness. The pre-metered thickness can be achieved in an operating space, referred to here as the *coating window*, which is bounded by various failure mechanisms. For example, the most prevalent and well-known failure mechanism is entrainment of air between the coated liquid and substrate, which places an upper limit on the coating speed in all coating methods. In general, coating has developed as an empirical art, although many of these methods and their failure mechanisms are understood scientifically—or at least well enough that sound engineering judgments can be made. For a general review of coating methods and known scientific principles, see the comprehensive book by Kistler and Schweizer (1997) and the review article of Weinstein and Ruschak (2004).

Ruschak (1976) provides perhaps the simplest and most elegant coating window in his examination of slot coating. In this method, a liquid bridge, often referred to as a *coating bead*, fills a narrow gap L between the coating die and a substrate moving at speed V_s to create a film of thickness d (Fig. 1). Ruschak considers the flow of Newtonian liquids in which gravitational and inertial effects are negligible and capillary effects dominate. The flow configuration is assumed to be two-dimensional and therefore invariant with the distance perpendicular to Fig. 1. For a liquid of viscosity, μ, and density, ρ, in the presence of gravity, g,

* Corresponding author. Tel.: +1 585 722 0490; fax: +1 585 722 5387.
E-mail address: steven.weinstein@kodak.com (S.J. Weinstein).

0009-2509/$ - see front matter © 2005 Elsevier Ltd. All rights reserved.
doi:10.1016/j.ces.2005.04.073

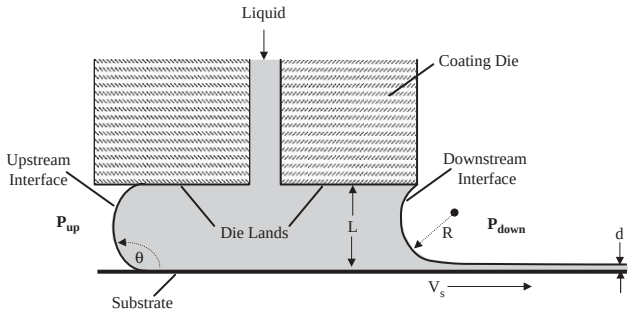

Fig. 1. Side view schematic of a typical slot-coating geometry. The liquid filling the gap between the die lands and the substrate, as well as the bounding interfaces, are often collectively referred to as a "coating bead."

this flow regime is characterized by small capillary numbers, $Ca = \mu V_s/\sigma$, small Bond numbers, $Bd = \rho g L^2/\sigma$, and small Reynolds numbers, $Re = \rho V_s d/\mu$. In this limit, the two interfaces that bound the bead are essentially circular, and serve to hold the bead in place. As a result, the coating window can be examined geometrically, where coating failures occur when either the upstream or downstream interface cannot be constructed that bridges the gap. For a Newtonian liquid, the constant radius of curvature of the downstream interface, R, is set from the Landau–Levich relation (Levich, 1962) according to $d/R = 1.34Ca^{2/3}$. In the low Ca approximation, $d/R \ll 1$, and the downstream interface appears on the scale of the gap, L, to intersect the web so that the angle of intersection is 0° (measured within the liquid); consequently, coating failure occurs when $R < L/2$, which limits the coating speed in dimensional form. Provided the downstream interface may be constructed, the Young–Laplace equation sets the pressure in the liquid relative to the ambient air pressure, P_{down}, applied along the face of the downstream interface in Fig. 1. The liquid pressure directly adjacent to the downstream interface is imposed on the liquid side of the *upstream* interface, as the low Ca approximation precludes pressure variations in the liquid due to motion. The upstream interface must then be constructed so that it is pinned at the slot exit, meets the substrate at a specified dynamic contact angle, θ, and has a radius of curvature again dictated by the Young–Laplace equation.The pressure applied along the air face of the upstream interface, P_{up}, thus largely affects this radius. Ruschak shows that an ambient pressure difference across the bead, satisfying $P_{\text{up}} - P_{\text{down}} < 0$, is generally required to coat as thin and fast as possible; this negative pressure difference is often referred to as suction. Failure modes of the upstream interface therefore accompany the application of too high or too low suction that precludes its geometric construction.

Ruschak's basic theory has been expanded by others to include the effects of gravity and viscosity created by the flow between the lands of the die and the substrate (Fig. 1), as well as die geometries in which the lands are not parallel to the substrate (Higgins and Scriven, 1980). Additionally, Carvalho and Kheshgi (2000) have examined the inclusion of inertial effects by replacing the Landau–Levich relation with a height-averaged form of the boundary layer equations governing thin film flows with moderate inertia (Kheshgi, 1989; Kheshgi et al., 1992). Hens and Boiy (1986) and Carvalho and Kheshgi (2000) further propose that there is a coupling between the upstream and downstream interfaces that is due to a boundary layer along the substrate at higher speeds. These complications typically serve to change the quantitative predictions of Ruschak's model, but they do not affect the qualitative geometrical character of the predicted gross failures described above. Ruschak's model explains typical experimental observations of at least two gross failures found, regardless of flow regime—too little suction causes the bead to break into dry patches, and too much suction pulls a portion of the bead into the vacuum chamber (Kistler and Schweizer, 1997). Even with the above-cited extensions of Ruschak's theory, the flow regime is still limited to interface shapes that are approximately circular, so *Ca*, *Re*, and *Bd* need to be small; thus the physics is surface-tension dominated. In other regimes, finite element predictions have been used to examine slot coating (see, for example, Saito and Scriven, 1981; Sartor, 1990; Carvalho and Kheshgi, 2000).

Regardless of the degree of sophistication in any model or simulation, quantitative comparisons with experiment are often confounded by the fact that it is possible for the upstream and downstream interfaces to pin at various locations along the lands of the die. Furthermore, none of these theories are capable of predicting the value of the dynamic contact angle as well as air entrainment at high speeds, which often occurs when the contact angle approaches 180°; these need to be empirically determined and depend on the nature of the interaction between the substrate, liquid, and air–liquid properties. Another common gross failure, ribbing (Kistler and Schweizer, 1997)—a hydrodynamic instability that destroys the two-dimensional nature of a coating by creating a regular lengthwise pattern of streaks—arises in diverging slot geometries in the direction of flow, and it is only predictable via auxiliary stability analyses based on assumed locations of the interface pinning points and dynamic contact angle. It is therefore often examined experimentally as well. These, and other constraints, can further limit the allowable parameter ranges and applicability of a predicted coating window.

The alternative extremely viscous coating regime, as characterized by $Ca \gg 1$ and $Re \ll 1$, has been studied primarily in the context of film casting processes. Here, a highly viscous melted polymer is extruded through a die to form a two-dimensional planar liquid sheet, which falls vertically through the air and impinges on a chilled roll to create a solid sheet. Yeow (1974) provided the first theoretical analysis of both the steady-state flow and stability of this planar configuration for a Newtonian liquid, which is analogous to previous work done on the melt spinning of polymer fibers (Matovich and Pearson, 1969). Yeow's model treats the planar sheet as gradually thinning in the direction of flow; to be consistent with this assumption, end effects near the slot (e.g., die swell) and substrate are not included (Matovich

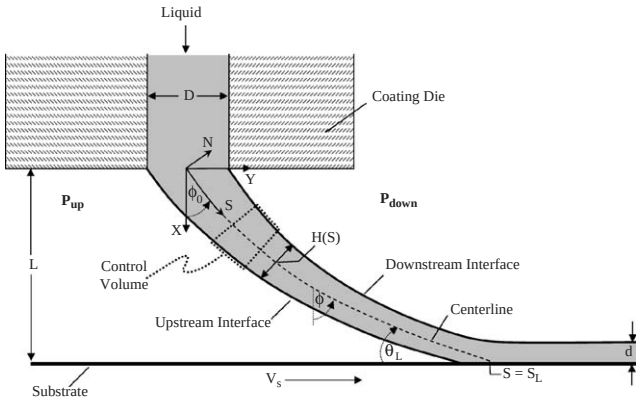

Fig. 2. Side view schematic of a typical extrusion coating geometry indicating coordinate system and physical parameters used in the analysis of the extruded liquid sheet.

and Pearson, 1969). An analytical expression for the velocity field and shape of the liquid interfaces is derived. Aird and Yeow (1983) extend this analysis to power-law liquids, and analogous steady-state analytical expressions are derived. Later works by Anturkar and Co (1988) and Iyengar and Co (1993) examine more sophisticated viscoelastic liquids using non-analytical methods. In all of these works, the width of the film is assumed to be constant and the film shape two-dimensional, when in fact the sheet width reduces significantly from the slot to the chill roll. This neck-in, and the concomitant edge thickness variation in the cast film, is predicted theoretically for Newtonian (D'Halewyu et al., 1990; Sakaki et al., 1996) and viscoelastic liquids (Silgay et al., 1998; Satoh, 2001), and is clearly observed experimentally (Dobroth and Erwin, 1986; Canning and Co, 2000).

A less-studied configuration, still within the confines of a viscous-dominated regime, is a small space occurring between the die and the substrate. This configuration is referred to as extrusion coating, and is distinguished from slot coating described above (see Chapter 11a of Kistler and Schweizer, 1997). In contrast to slot coating in which liquid often wets the lands of the die (Fig. 1), extrusion coating actually invokes a short two-dimensional liquid sheet that bridges the gap where the sheet only contacts the die at the slot exit (Fig. 2). The space between the die and substrate can be larger than that in slot coating because capillarity is not required to support the liquid bead. Instead, the liquid sheet in extrusion coating is held in the space between the die and substrate by the traction along the substrate and the slot. Despite the narrow gap, this sheet will often be dragged so that it is still relatively long compared with its thickness. Furthermore, with a small die-to-substrate spacing and a large width, the relative extent of the reduction in width of the liquid sheet, as cited in the film casting literature above, will be small.

The preceding arguments suggest that a constant-width, two-dimensional model of a gradually thinning sheet can supply a reasonable approximation to the flow field in an extrusion coating operation. Ding et al. (2000, 2001) model the flow of this geometry, although they use an ad hoc assumption about the form of the velocity field. Furthermore, their derived model of the sheet does not reduce to that of Yeow (1974) and Aird and Yeow (1983) when the sheet is vertical. This calls into question the validity of the analyses of Ding et al. (2000, 2001), because the steady-state Newtonian sheet equations of Yeow (1974) agree precisely with those derived via asymptotic methods by Van De Fliert et al. (1995) and Ramos (1996) for a viscous-dominated sheet that is gradually thinning. These results are also limiting cases of more general asymptotic analyses of two-dimensional gradually thinning liquid sheets involving inertia, gravity, and viscous effects (Clarke, 1968; Ramos, 1996), generally referred to as "curtains" in the coating literature (Kistler and Schweizer, 1997). These asymptotic liquid sheet equations agree with those first derived using physical arguments by Taylor in the appendix of Brown (1961), who also verified the result experimentally, and have also been experimentally verified in the inviscid limit (Finnicum et al., 1993; Weinstein et al., 1997; Clarke et al., 1997). Again, as in the film casting work cited above, end effects are neglected for all of the derived liquid sheet equations. Note that Ding et al. (2000, 2001) do not examine the effect of a pressure drop applied across the thin sheet, which might be anticipated to affect the size of the coating window as in the low capillary number cases cited previously.

In this paper, we determine the steady-state operating window for extrusion coating in the presence of applied pressures, and we explore the shape of the two-dimensional, thin viscous sheet between the slot and the substrate for a power-law liquid. The organization of this paper is as follows. Section 2 provides the theoretical analysis of the coating configuration. In Section 2.1, the boundary-value problem to determine the shape of the liquid sheet is set forth, and an analytical solution is provided in Section 2.2. An analytical expression for the extrusion coating window is determined in Section 2.3 via geometrical construction in a way directly analogous to the above-cited work of Ruschak (1976). Theoretical results are provided in Section 3, and a discussion is provided in Section 4. The main text closes in Section 5 with a summary. Appendix A provides a derivation of the steady equations governing the shape of a gradually thinning planar sheet in the presence of a pressure drop via a macroscopic balance on the control volume, indicated in Fig. 2; this generalizes the above-cited asymptotically valid equations to non-vertical configurations. Appendix B provides an analytical expression for the viscosity dependence and average viscosity in the liquid sheet.

2. Theory

2.1. Boundary value problem for the extruded sheet

We now develop a well-posed boundary value problem to solve for the liquid sheet in extrusion coating, which we will

refer to as the *extruded sheet*. To this end, consider the configuration shown in Fig. 2, which shows the extrusion coating geometry to be modeled. Here, liquid of density ρ exits a coating die with a slot of height D and an imposed volumetric flow rate per unit width Q to form a two-dimensional extruded sheet that is invariant with distance perpendicular to the plane of Fig. 2. The air–liquid interfaces bounding the sheet are assumed to have a constant surface tension σ. The extruded sheet is pulled by a substrate moving at speed V_s across a gap of distance L. The dynamics of the ambient air is neglected, although different pressures may be applied on the upstream and downstream faces of the extruded sheet denoted by P_{up} and P_{down}, respectively.

An S–N coordinate system is oriented as indicated in Fig. 2, where S and N denote the respective distances along the centerline and normal to the extruded sheet. An auxiliary X–Y coordinate system, also shown in Fig. 2, is related to the S–N system in terms of the angle ϕ between the tangent to the centerline and the vertical X-axis as

$$\frac{\mathrm{d}X}{\mathrm{d}S} = \cos\phi, \quad \frac{\mathrm{d}Y}{\mathrm{d}S} = \sin\phi. \tag{1}$$

The local thickness of the sheet is parameterized as $H(S)$, where the downstream and upstream interfaces are located at $N = H(S)/2$ and $N = -H(S)/2$, respectively. The sheet is assumed to thin gradually in the direction of flow, and it is therefore anticipated that the streamwise velocity component, U, is essentially invariant with N, and can thus be parameterized as $U(S)$. The liquid obeys a power-law constitutive equation $\boldsymbol{\tau} = \eta\boldsymbol{\gamma}$, where $\boldsymbol{\tau}$ is the stress tensor, $\boldsymbol{\gamma}$ is the rate of strain tensor, and η is the shear-dependent viscosity; this viscosity can be expressed as $\eta = m|\gamma|^{n-1}$, where m is the consistency coefficient, n is the power-law exponent, and the vertical lines denote magnitude. In this paper, we restrict attention to either Newtonian ($n = 1$) or shear thinning ($n < 1$) liquids. A derivation of the general mass conservation and force equations for a power-law liquid sheet is provided in Appendix A using macroscopic balances; these equations are consistent with all asymptotically correct equations for gradually thinning sheets cited in Section 1.

The assumption of a gradually thinning liquid sheet is not valid in the vicinity of the slot and substrate because the flow in the S and N directions are comparable. Thus, as in the literature cited in Section 1, end effects are neglected in these regions. The slot boundary conditions are thus applied at the location $S = 0$, where it is assumed that $U = Q/D$ and $H = D$. The length of the centerline is denoted by S_L, which is determined as part of the solution of the problem. The angle of intersection between the sheet centerline and the substrate at $S = S_L$, denoted as θ_L, is specified (Fig. 2). It is also assumed that liquid at the bottom of the extruded sheet moves at the speed of the substrate, which is resolved along the tangent to the centerline, i.e., $V_s \cos\theta_L$. We require that $V_s \cos\theta_L > Q/D$ in our analysis, so that the film is stretched and thinned by the moving substrate—this is typically the industrially relevant situation. A discussion of the validity of these assumed boundary conditions, and the implications of the neglected end effects, is provided in Section 4.

Dependent and independent variables are made dimensionless as follows:

$$s = \frac{S}{L}, \quad x = \frac{X}{L}, \quad y = \frac{Y}{L},$$
$$u = \frac{UD}{Q}, \quad h = \frac{H}{D}. \tag{2a}$$

Upon substitution of Eq. (2a) into the governing equations and boundary conditions, the following dimensionless groups are obtained:

$$Re = \frac{\rho Q L}{D\eta^*}, \quad Ca = \frac{\eta^* Q}{L\sigma}, \quad G = \frac{\rho g D L^2}{\eta^* Q},$$
$$v_s = \frac{V_s D}{Q}, \quad p_{\text{down}} = \frac{P_{\text{down}} L^2}{Q\eta^*}, \quad p_{\text{up}} = \frac{P_{\text{up}} L^2}{Q\eta^*}. \tag{2b}$$

In Eq. (2b), g is the gravitational constant, and the viscosity scale, η^*, is defined in terms of parameters of the assumed power-law relation as

$$\eta^* = m\left(\frac{Q}{DL}\right)^{n-1}. \tag{2c}$$

This scale is justified by inspection of the functional form of the viscosity, which is simplified for a gradually thinning film, as given by Eq. (A.3b).

As evident in the dimensionless form of the general force equation, Eq. (A.6), derived in the appendix, the first three parameters, Re, Ca, and G determine the magnitude of inertia, surface tension, and gravitational forces compared with viscous forces. For typical extrusion coating conditions associated with a small gap spacing L, $Re \ll 1$, $Ca \gg 1$ and $G \ll 1$. Under these circumstances, viscous and pressure forces dominate all others, and the limiting form of the force equation, Eq. (A.6), for the extruded sheet become

$$\frac{\mathrm{d}}{\mathrm{d}s}\left(h\left[\frac{\mathrm{d}u}{\mathrm{d}s}\right]^n\right) = 0, \tag{2d}$$

$$4^n h\left(\frac{\mathrm{d}u}{\mathrm{d}s}\right)^n \frac{\mathrm{d}\phi}{\mathrm{d}s} = p_{\text{down}} - p_{\text{up}}. \tag{2e}$$

The mass balance in the sheet Eq. (A.1) is given in dimensionless form as

$$\frac{\mathrm{d}(uh)}{\mathrm{d}s} = 0. \tag{2f}$$

We note here that for a Newtonian liquid (where $n = 1$, and m is interpreted as the viscosity) Eqs. (2d–f) are identical to those derived by Van De Fliert et al. (1995) under steady-state conditions. The dimensionless boundary conditions are:

$$u = 1, \quad h = 1 \quad \text{at } s = 0, \tag{2g}$$

$$u = v_s \cos\theta_L, \quad \phi = \frac{\pi}{2} - \theta_L \quad \text{at } s = \frac{S_L}{L} \equiv s_L. \tag{2h}$$

A constraint on the length of the extruded sheet is derived from Eq. (1) as

$$\int_0^{s_L} \cos\phi \, \mathrm{d}s = 1. \tag{2i}$$

The system Eq. (2) is well posed to determine the shape of the extruded sheet's centerline, $\phi(s)$, its local thickness, $h(s)$, and internal speed $u(s)$. Note that the system, Eq. (2) is general for an arc-length-dependent pressure drop, but we restrict attention in this paper to cases where $p_{\mathrm{down}} - p_{\mathrm{up}}$ in Eq. (2e) is constant.

Once solved, the x–y-coordinates of the extruded sheet's centerline can be extracted by integrating Eq. (1) to obtain

$$x_c = \int_0^s \cos\phi \, \mathrm{d}s, \quad y_c = \int_0^s \sin\phi \, \mathrm{d}s, \tag{3a}$$

where the subscript "c" has been added to denote the centerline location. The position of the downstream and upstream interfaces are obtained by relating the X–Y and S–N coordinate systems in Fig. 2 to yield

$$x = x_c \mp \frac{1}{2}\delta h \sin\phi, \quad y = y_c \pm \frac{1}{2}\delta h \cos\phi, \quad \delta = \frac{D}{L}, \tag{3b}$$

where the upper and lower signs correspond to the downstream and upstream interfaces, respectively.

2.2. Solution for the shape of the extruded sheet

The solution of the system, Eq. (2) is now obtained. Eq. (2f) is integrated and the boundary conditions, Eq. (2g), are applied to yield:

$$h = \frac{1}{u}. \tag{4}$$

Eq. (2d) is integrated to yield:

$$h\left[\frac{\mathrm{d}u}{\mathrm{d}s}\right]^n = \alpha, \tag{5}$$

where α is a constant to be determined. Substituting Eq. (4) into Eq. (5) and using the speed boundary condition in Eq. (2h), the result is

$$u = \begin{bmatrix} \left(1 + \frac{(n-1)}{n}\,\alpha^{1/n} s\right)^{n/(n-1)}, & \text{for } n < 1 \\ e^{\alpha s}, & \text{for } n = 1 \end{bmatrix}, \tag{6a}$$

where

$$\alpha = \begin{bmatrix} \left(\frac{n(1-[v_s\cos\theta_L]^{(n-1)/n})}{(1-n)s_L}\right)^n, & \text{for } n < 1 \\ \frac{\ln(v_s\cos\theta_L)}{s_L}, & \text{for } n = 1 \end{bmatrix}. \tag{6b}$$

A constraint on the velocity field that is evident in Eq. (6b) for $n < 1$, is that:

$$v_s \cos\theta_L \geqslant 1. \tag{6c}$$

This mathematical restriction arises because we have limited attention to cases of thinning extruded sheets where $\mathrm{d}u/\mathrm{d}s > 0$; see Appendix A for a more general governing equation, which is not subject to this restriction. Note that the velocity result, Eq. (6a), is consistent with derived analytical expressions for both Newtonian and power-law liquids for the special case of a vertical sheet (Yeow, 1974; Aird and Yeow, 1983). An interesting analytical feature of the velocity field, Eq. (6), is that it yields a viscosity variation that is linear with arc length along the sheet when $n < 1$. A derivation of this result, and an expression for the average viscosity in the extruded sheet, are provided in Appendix B.

The velocity field, Eq. (6), is in terms of a not-yet-known length of the extruded sheet, s_L, which is determined in the following. The expression in Eq. (5) is substituted into Eq. (2e) and rearranged to yield

$$\frac{\mathrm{d}\phi}{\mathrm{d}s} = \frac{p_{\mathrm{down}} - p_{\mathrm{up}}}{4^n \alpha} \equiv \kappa. \tag{7}$$

This result indicates that the interface shape is circular with dimensional curvature κ/L. After integration of Eq. (7), and application of the angle boundary condition in Eq. (2h), the result is

$$\phi = \kappa(s - s_L) + \frac{\pi}{2} - \theta_L. \tag{8a}$$

The result, Eq. (8a), is in turn substituted into Eq. (2i) to obtain the following equation that can be solved to determine the arc length, s_L:

$$\cos(\theta_L + \kappa s_L) = \cos\theta_L - \kappa \tag{8b}$$

Once Eq. (8b) is satisfied, the solution to the system of Eq. (2) is complete.

The Cartesian coordinates of the centerline can be extracted by substituting Eq. (8a) into Eq. (3a) to yield

$$x_c = \kappa^{-1}(\cos[\theta_L + \kappa\{s_L - s\}] - \cos[\theta_L + \kappa s_L]), \tag{8c}$$

$$y_c = \kappa^{-1}(\sin[\theta_L + \kappa s_L] - \sin[\theta_L + \kappa\{s_L - s\}]). \tag{8d}$$

The locations of the downstream and upstream interfaces are obtained from Eq. (3b) as

$$x = x_c \mp \tfrac{1}{2}\delta h \cos[\theta_L + \kappa\{s_L - s\}], \tag{8e}$$

$$y = y_c \pm \tfrac{1}{2}\delta h \sin[\theta_L + \kappa\{s_L - s\}], \tag{8f}$$

where δ is defined in Eq. (3b). The result, Eq. (8), provides a complete description of the shape of the extruded liquid sheet.

2.3. The extrusion coating window

Of particular interest is the parameter space in which extrusion coating is possible (i.e., the coating window) when

a pressure drop is applied across the extruded sheet. Extrusion coating is possible when the circular shape of the extruded sheet—subjected to the constraints that it is pinned at the slot, meets the imposed angle at the substrate, and has a specified radius of curvature—can bridge the gap between the slot and the substrate. This parallels the geometrical construction and associated operability bounds for the upstream interface in slot coating (Fig. 1), as elucidated by Ruschak (1976) in surface tension-dominated flows, which also involve circular interface shapes.

To obtain bounds, attention is focused in Eq. (8b). The maximum and minimum values of the cosine function on the left-hand side are 1 and −1, respectively, which sets limiting values of the curvatures at $\pm 1 = \cos\theta_L - \kappa$. The arc lengths associated with these limiting values are obtained by choosing the appropriate branch for the argument of the cosine on the left-hand side that is consistent with the physical construction of a circle. The result is

$$\kappa_1 = \cos\theta_L - 1, \quad s_{L1} = \frac{\theta_L}{1-\cos\theta_L}, \tag{9a}$$

$$\kappa_2 = \cos\theta_L + 1, \quad s_{L2} = \frac{\pi-\theta_L}{1+\cos\theta_L}, \tag{9b}$$

where the subscripts have been added to κ and s_L for later reference. Note that all curvatures must lie in the range

$$\kappa \in [\kappa_1, \kappa_2]. \tag{9c}$$

Furthermore, the sense of the curvatures is different in the two limiting cases. The curvature in Eq. (9a) is generally negative, and that for Eq. (9b) is positive. According to the expression for the surface angle ϕ given in Eq. (7), a negative curvature implies that the circular centerline is curved so that its center lies to the left of the extruded sheet in Fig. 2, and the positive radius implies that its center lies to the right.

With the critical radii identified, we can now identify the range of pressure drops that can be supported by the extruded sheet. Rearrangement of Eq. (7) to solve for the pressure drop in Eq. (9) yields the following inequality:

$$\Delta p_{\min} \leqslant p_{\text{down}} - p_{\text{up}} \leqslant \Delta p_{\max}, \tag{10a}$$

where

$$\Delta p_{\min} \equiv 4^n \alpha\kappa|_1, \quad \Delta p_{\max} \equiv 4^n \alpha\kappa|_2 \tag{10b}$$

and the subscripts 1 and 2 indicate that α and κ in each limit correspond to the critical locations in Eq. (9). Explicit evaluation of Eq. (10b), using Eqs. (6b) and (9), yields

$$\Delta p_{\min} = \begin{bmatrix} 0, & \text{for } \theta_L = 0 \ \forall n \\ -(1-\cos\theta_L)^{n+1}\left(\frac{4n(1-[v_s\cos\theta_L]^{(n-1)/n})}{(1-n)\theta_L}\right)^n, & \text{for } n<1 \\ -\frac{4(1-\cos\theta_L)^2}{\theta_L}\ln(v_s\cos\theta_L), & \text{for } n=1 \end{bmatrix} \tag{10c}$$

$$\Delta p_{\max} = \begin{bmatrix} (1+\cos\theta_L)^{n+1}\left(\frac{4n(1-[v_s\cos\theta_L]^{(n-1)/n})}{(1-n)(\pi-\theta_L)}\right)^n, & \text{for } n<1 \\ \frac{4(1+\cos\theta_L)^2}{\pi-\theta_L}\ln(v_s\cos\theta_L), & \text{for } n=1 \end{bmatrix}, \tag{10d}$$

where, for ease of later reference, we rewrite the assumed constraint Eq. (6c) here as

$$v_s\cos\theta_L \geqslant 1. \tag{10e}$$

The dimensionless inequality in Eq. (10) provides the range of applied pressures in which the extruded sheet can bridge the gap between the slot and moving substrate, and thus describes the parameter space in which extrusion coating is possible.

3. Results

We begin our discussion by examining the centerline deflection of the extruded liquid sheet. Eqs. (6b) and (7) indicate that the curvature κ of the sheet centerline is a function of not only the pressure drop $p_{\text{down}} - p_{\text{up}}$, but of the power-law exponent n, angle of intersection with the substrate θ_L, and dimensionless speed of the substrate v_s. However, Eq. (8b) indicates that it is permissible to alternatively *specify* κ and θ_L, solve for s_L, and extract centerline shapes according to Eqs. (8c) and (8d). This is convenient for data presentation because all combinations of $p_T - p_B$, n, and v_s, which give the same value of the curvature for given θ_L, will yield the same centerline prediction; therefore, the range of possible centerline shapes can be explored in an efficient way. Fig. 3 gives typical centerline shapes for $\theta_L = 10°$ over the range of possible curvatures that allow a circular arc to be constructed according to Eqs. (9). Note that $x = 0$ and 1 correspond to the locations of the slot and substrate, respectively. Curves **A** and **F** correspond to limiting curvatures $\kappa_2 = 1.985$ and $\kappa_1 = -0.0152$, and curves **B**–**E** correspond to intermediate values. Note that curve **D** corresponds to the

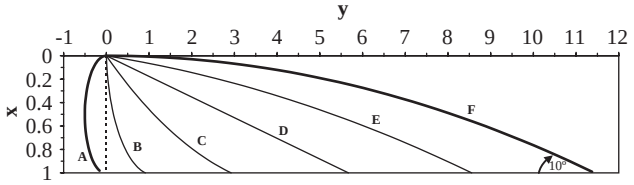

Fig. 3. Coordinate plot showing the effect of curvature, κ, on the centerline shape of the extruded liquid sheet for $\theta_L = 10°$. (A) Maximum curvature, $\kappa = \kappa_2 = 1.985$; (B) $\kappa = 0.9$; (C) $\kappa = 0.1$; (D) $\kappa = 0$; (E) $\kappa = -0.0135$; (F) minimum curvature, $\kappa = \kappa_1 = -0.0152$.

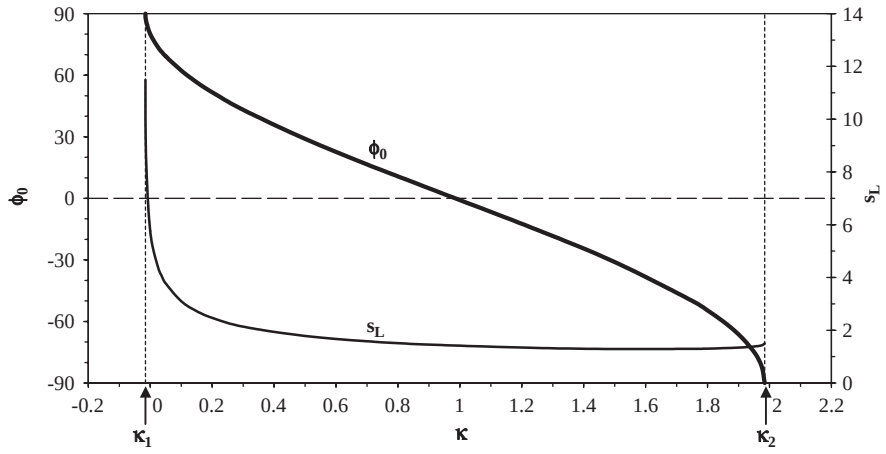

Fig. 4. Plots of the angle of the extruded sheet's centerline at the slot relative to vertical, ϕ_0, expressed in degrees, and the arc length of the centerline, s_L, as a function of the curvature, κ, of the centerline for $\theta_L = 10°$. This plot encompasses the range of curvatures and associated centerline shapes examined in Fig. 3. The indicated minimum and maximum allowable curvatures have respective values of $\kappa_1 = -0.0152$ and $\kappa_2 = 1.985$.

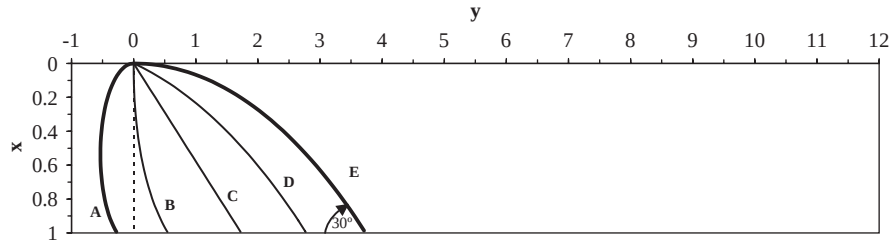

Fig. 5. Coordinate plot showing the effect of curvature, κ, on the centerline shape of the extruded liquid sheet for $\theta_L = 30°$. (A) Maximum curvature, $\kappa = \kappa_2 = 1.866$; (B) $\kappa = 0.9$; (C) $\kappa = 0$; (D) $\kappa = -0.12$; (E) minimum curvature, $\kappa = \kappa_1 = -0.134$.

case of zero curvature and serves as a dividing line separating positive curvatures (curves **A**–**C**) and negative curvatures (curves **E**–**F**). It is also apparent that the arc length s_L of the extruded sheet increases as its curvature is reduced, as expected from physical intuition.

As is evident from inspection of Fig. 3, the centerline of the extruded sheet does not, in general, exit the slot (at $x = y = 0$) vertically. The angle of the centerline at the slot, relative to vertical, denoted as ϕ_0 (Fig. 2), is obtained directly from Eq. (8a) evaluated at $s = 0$:

$$\phi_0 = -\kappa s_L + \frac{\pi}{2} - \theta_L. \tag{11}$$

Fig. 4 provides a plot of the angle ϕ_0 from Eq. (11) as well as the arc length of the centerline, s_L, as a function of curvature κ for $\theta_L = 10°$; this figure encompasses the variation in ϕ_0 and s_L associated with all of the centerline predictions of Fig. 3. Fig. 4 indicates that the angle ϕ_0 decreases monotonically with increasing curvature in the range of the limiting configurations. Note that curves **A** and **F** in Fig. 3 correspond to the limiting configurations κ_2 and κ_1 shown in Fig. 4, and have $\phi_0 = -90°$ and $\phi_0 = 90°$, respectively. This result is general to all limiting configurations, regardless of parameter values. Fig. 4 indicates that the arc length decreases monotonically with increasing curvature, except in the immediate vicinity of the limiting configuration κ_2. Additionally, Fig. 4 indicates that the arc length is a strong function of curvature for small values of curvature close to κ_1.

Figs. 5 and 6 give analogous data to Figs. 3 and 4, except for $\theta_L = 30°$. Curves **A** and **E** in Figs. 5 and 6 correspond respectively to limiting curvatures $\kappa_2 = 1.866$ and $\kappa_1 = -0.134$, and curves **B**–**D** in Fig. 5 correspond to intermediate values. Comparisons between Figs. 4 and 6 indicate that arc lengths for the same values of curvatures, in the range of admissible values, are smaller when $\theta_L = 30°$. Nevertheless, the same general trends are observed when $\theta_L = 30°$ and $10°$.

Although centerline shapes can be conveniently examined in the space of κ and θ_L, the local velocity and film thickness centered about the centerline are strong functions of n and v_s. Figs. 7 and 8 show the effect of power-law exponent, n, on respective speed and thickness predictions Eqs. (6) and (4) with $v_s = 6$, for a centerline shape characterized by $\theta_L = 10°$ and $\kappa = 0.9$. Note that the centerline shape for all values of n in either figure is identical and is shown in curve **B** of Fig. 3; this shape gives $s_L = 1.46$ and $\phi_0 = 4.87°$ from Fig. 4. In Figs. 7 and 8, the arc-length coordinates in Eq. (6) is transformed to x (the vertical distance from the

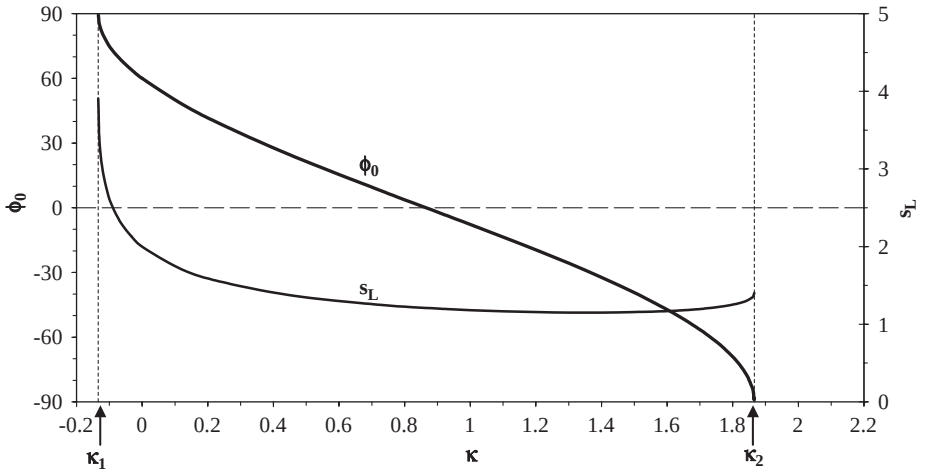

Fig. 6. Plots of the angle of the extruded sheet's centerline at the slot relative to vertical, ϕ_0, expressed in degrees, and the arc length of the centerline, s_L, as a function of the curvature, κ, of the centerline for $\theta_L = 30°$. This plot encompasses the range of curvatures and associated centerline shapes examined in Fig. 5. The indicated minimum and maximum allowable curvatures have respective values of $\kappa_1 = -0.134$ and $\kappa_2 = 1.866$.

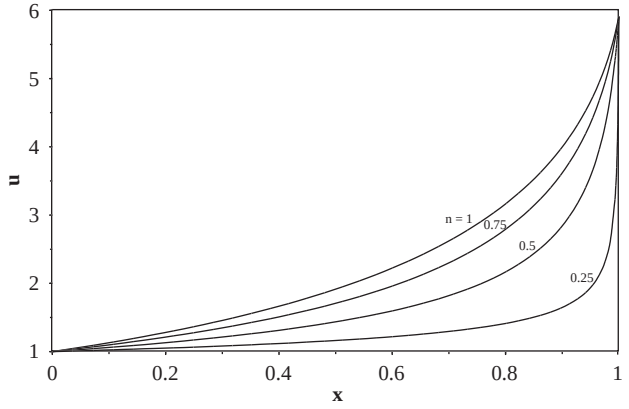

Fig. 7. Speed of liquid in the extruded sheet, u, as a function of linear distance from the slot, x, for various power-law exponents, n. All curves have $\theta_L = 10°$ and $\kappa = 0.9$, and correspond to extruded sheets having the same centerline shape given by curve **B** in Fig. 3.

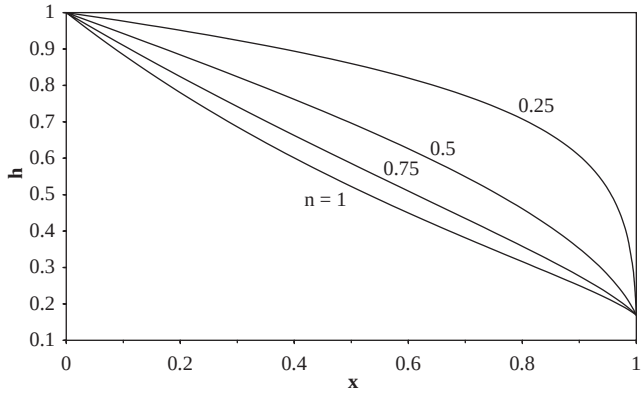

Fig. 8. Thickness of the extruded sheet, h, as a function of linear distance from the slot, x, for various power-law exponents, n, associated with fluid speeds in Fig. 7. All curves have $\theta_L = 10°$ and $\kappa = 0.9$, and correspond to extruded sheets having the same centerline shape given by curve **B** in Fig. 3.

slot in Fig. 2) through the centerline expression Eq. (8c). Figs. 7 and 8 show that the velocity and film thicknesses are monotonic with distance from the slot; it is apparent that as n decreases, much of the speed and thickness variation occurs in the extruded sheet near the substrate.

Fig. 9 gives a complete shape of the extruded sheet corresponding to the velocity and thickness profiles in Figs. 7 and 8 for a Newtonian liquid ($n = 1$), where the local sheet thickness of Fig. 8 has been superimposed on the centerline shape, according to Eqs. (8e) and (8f) for $\delta = 0.1$. The centerline location in Fig. 9 is dashed, and the angle of the centerline at its top is $\phi_0 = 4.86°$. Fig. 9 shows that the film thickness dips below the substrate location at $x = 1$. We could have chosen to ignore this portion of the solution in our plot, which is clearly not physical. However, here, we have elected to include this deviation to illustrate that our analysis ignores end effects; thus, it is unaware of the physical constraint of the substrate apart from the speed and angle imposed on the centerline.

Fig. 10 gives a comparison between the shape of the Newtonian and power-law liquid sheets corresponding, respectively, to $n = 1$ and 0.25 from Figs. 7 and 8; the Newtonian interface shape, indicated with thin solid lines, is identical to that shown in Fig. 9. It is again emphasized that the curvature κ and angle θ_L are identical for both liquids; therefore, the centerline shape, indicated with the small dashes in the figure, is the same in both cases. Fig. 10 shows that the extruded sheet is thicker for a power law liquid at each location, and it rapidly thins in the vicinity of the substrate to meet the constraints of imposed angle and speed at that location. This is in accordance with the thickness and velocity behaviors observed in Figs. 7 and 8. Finally, Fig. 11

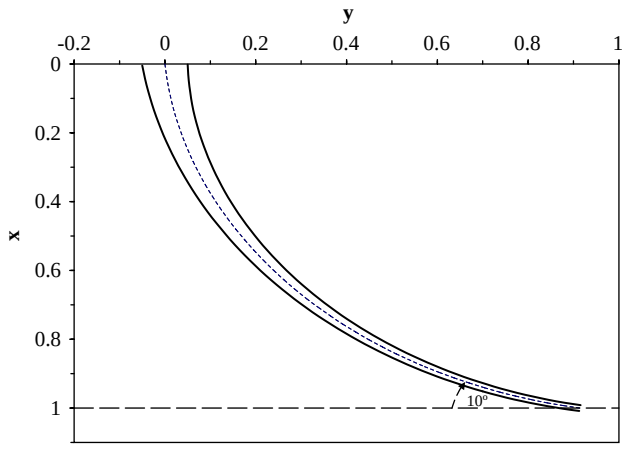

Fig. 9. Complete shape of the extruded sheet for a Newtonian liquid ($n=1$) for $\theta_L=10°$, $\kappa=0.9$, $v_s=6$ and $\delta=1$. The centerline corresponds to curve **B** of Fig. 3 and is indicated in small dashes. The associated speed and thickness data are found in Figs. 7 and 8.

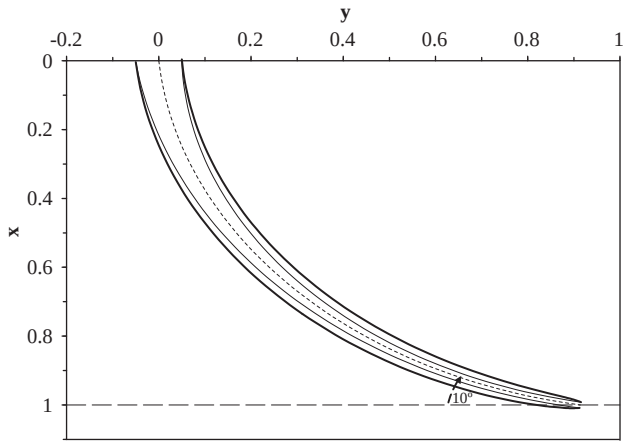

Fig. 10. Comparison of the complete shape of the extruded sheet for power-law ($n=0.25$) and Newtonian ($n=1$) liquids for $\theta_L=10°$, $\kappa=0.9$, $v_s=6$ and $\delta=1$. The location of interfaces for the power law and Newtonian liquids are indicated with dark and light solid lines, respectively. The Newtonian shape is identical to that in Fig. 9. The centerline for both cases is identical and indicated in small dashes, and corresponds to curve **B** of Fig. 3. The associated speed and thickness data are found in Figs. 7 and 8.

gives interface results for a Newtonian liquid, and parameter values identical to those in Fig. 9, except the angle is now $\theta_L=30°$ (thus, $\kappa=0.9$, $v_s=0.6$, $\delta=0.1$). Compared with Fig. 9, the arc length of the centerline is reduced to $s_L=1.201$, and the centerline shape is different (in agreement with trends shown in Figs. 3–6); despite this fact, a similar thinning shape is obtained.

We now turn our attention to typical predictions of coating windows according to Eq. (10). As is evident by inspection of Eq. (10), windows are functions of v_s, θ_L, and n. A more physical interpretation of v_s can be obtained by reconsidering its definition in Eq. (2b). For a pre-metered flow

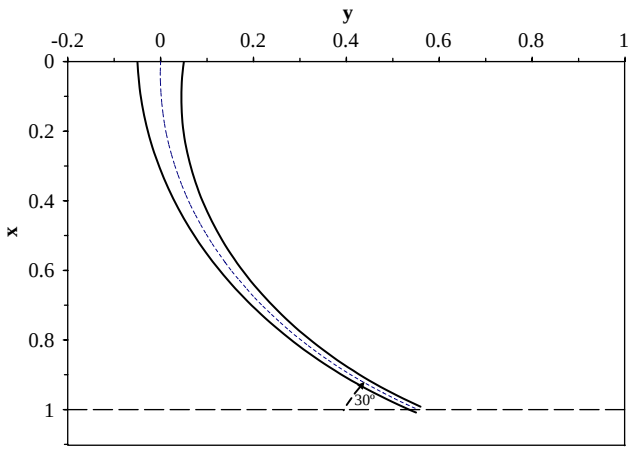

Fig. 11. Complete shape of the extruded sheet for a Newtonian liquid ($n=1$) for $\theta_L=30°$, $\kappa=0.9$, $v_s=6$ and $\delta=1$. The centerline corresponds to curve **B** of Fig. 5 and is indicated in small dashes.

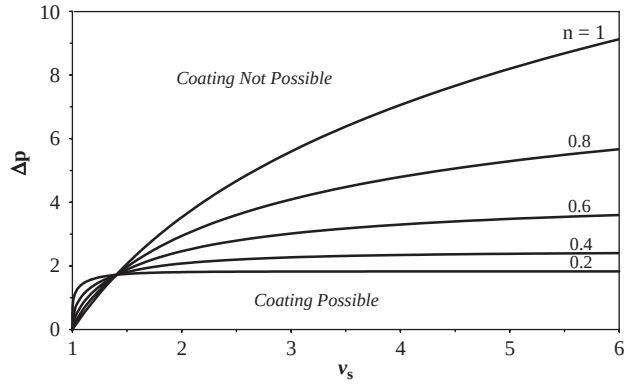

Fig. 12. Extrusion coating windows expressing the allowable range of pressure drops, $\Delta p = p_{\text{down}} - p_{\text{up}}$, as a function of the dimensionless thickness ratio, v_s, for various power-law exponents, n, and $\theta_L = 0°$.

on a horizontal surface, the dimensional final film thickness on the substrate, d (Fig. 2), is given by the plug relation $d=Q/V_s$, and thus v_s in Eq. (2b) is alternatively interpreted as a thickness ratio $v_s = D/d$. Fig. 12 gives coating windows for $\theta_L=0°$ expressing the range of allowable pressure drops across the liquid sheet, $\Delta p = p_{\text{down}} - p_{\text{up}}$, for various power-law exponents n as a function of the thickness ratio v_s. The curves shown for each value of n correspond to $\Delta p_{\max}$ in Eq. (10b); according to Eq. (10c), $\Delta p_{\min}=0$ when $\theta_L=0°$. Thus, the range of allowable pressure drops for a given power-law n lies between the indicated curve and the abscissa in Fig. 12. Note that the positive values of Δp within the window indicate that suction is applied to the upstream face of the liquid sheet, relative to the pressure applied to the downstream face (Fig. 2). As is evident from Fig. 12, regardless of the value of n, the window collapses when $v_s=1$, which is the smallest allowable value of v_s that satisfies Eq. (10e). Furthermore, for $n=1$, the size of the pressure window continues to increase with increasing v_s,

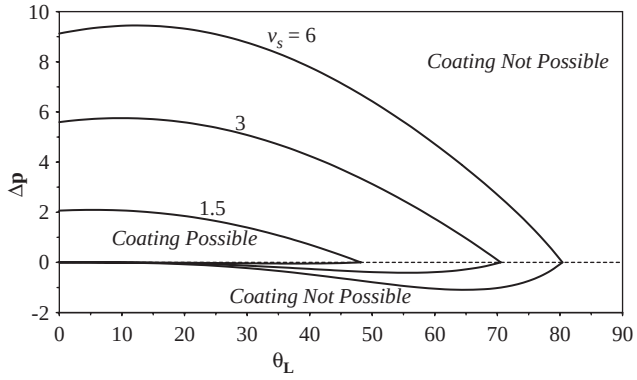

Fig. 13. Extrusion coating windows expressing the allowable range of pressure drops, $\Delta p = p_{\text{down}} - p_{\text{up}}$, as a function of the sheet angle at the substrate, θ_L, for various values of v_s and for a Newtonian liquid ($n = 1$).

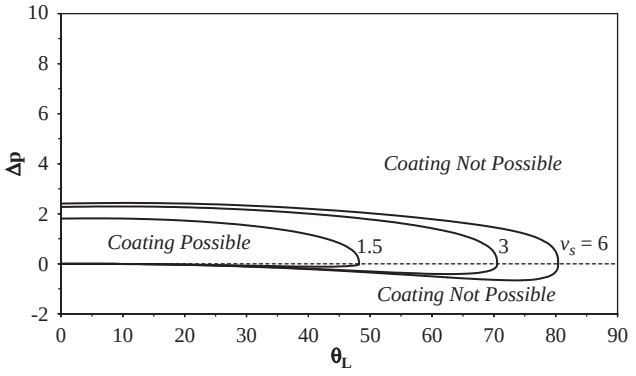

Fig. 14. Extrusion coating windows expressing the allowable range of pressure drops, $\Delta p = p_{\text{down}} - p_{\text{up}}$, as a function of the sheet angle at the substrate, θ_L, for various values of v_s and for $n = 0.4$.

which can also be deduced by direct inspection of Eq. (10d). For $n < 1$, however, all $\Delta p_{\max}$ curves ultimately asymptote to a constant value for large v_s, as evidenced by the curves for $n = 0.2$ and 0.4, although as $n \to 1$, the value of v_s required to reach this asymptote becomes large. The form of the limiting value for large v_s for any $n < 1$ is given by the expression in Eq. (10d) with terms involving v_s eliminated.

It is apparent that the smaller the value of n, the smaller the available window in Fig. 12. Note, however, that this is a statement made in the dimensionless space. The interpretation of this trend in dimensional form is confounded by the fact that the scales for pressure in Eq. (2b) involve n itself through the characteristic viscosity scale η^* in Eq. (2c). To see this explicitly, we rewrite Eq. (10a) in dimensional form using the pressure scaling in Eq. (2b) as

$$\left(\frac{Q\eta^*}{L^2}\right)\Delta p_{\min} \leqslant P_T - P_B \leqslant \left(\frac{Q\eta^*}{L^2}\right)\Delta p_{\max}. \tag{12}$$

From physical considerations for fixed geometry and flow, smaller values of n give smaller values of the characteristic viscosity scale; so the general trends shown in Fig. 12 also hold in the dimensional space. It is also apparent that the larger the characteristic viscosity for a given geometry, the larger the dimensional window.

Fig. 13 shows the dependence of the coating window on the angle θ_L for a Newtonian liquid and various thickness ratios v_s. Note that this figure is consistent with data for $\theta_L = 0$ from Fig. 12 for $n = 1$. Each of these windows collapses to a point for parameter values satisfying $v_s \cos\theta_L = 1$, the limit for which the thickness of the liquid no longer decreases in the direction of flow according to Eq. (10e). It is apparent that the magnitude of the dimensionless pressure latitude is relatively insensitive to angle for small values of θ_L for each thickness ratio. Note the appearance of negative values of the allowable pressure drop in Fig. 13 for larger angles; this indicates that it is now possible to maintain a liquid sheet when a positive pressure is applied along the upstream face of the liquid sheet, relative to the downstream face. Fig. 14 provides data analogous to that in Fig. 13, except now n=0.4. Because the values of v_s are the same in both Figs. 13 and 14, the values of the angles at which each window collapses (again corresponding to $v_s \cos\theta_L = 1$) are identical. As in the case of Fig. 13, note the relative insensitivity of the pressure window to angle variations for small angles. Dimensional Eq. (12) reveals that the pressure scaling (explicitly shown in parentheses) remains constant when fluid type, flow rate, and geometry are fixed. Thus, data trends in either Fig. 13 or 14 can be interpreted as corresponding to dimensional experiments in which the only parameters varied are the dimensional substrate speed V_s and intersection angle θ_L.

4. Discussion

We begin our discussion by extracting an important physical result from the solution for the extruded sheet given in Section 2.2. In particular, the form of Eq. (7), which gives a relation between pressure drop and the curvature of the sheet centerline, suggests that the liquid-extruded sheet experiences an effective dimensionless tensile force per unit width, σ_e, given as

$$\sigma_e = 4^n \alpha, \tag{13a}$$

where α is given by Eq. (6b). This interpretation is obtained by direct analogy to solid mechanics for a cylindrical shell of constant curvature subjected to a pressure drop, or alternatively, to the Young–Laplace equation for a pressure drop across a cylindrical interface with surface tension. The corresponding dimensional tensile force per unit width, σ^* is given as

$$\sigma_e^* = \left(\frac{\eta^* Q}{L}\right)\sigma_e, \tag{13b}$$

where η^* is given by Eq. (2c). According to Eq. (6), the parameter $\alpha > 0$, and thus Eq. (13) indicates that the extruded sheet is in a state of isotropic tension; this is an intuitively pleasing result consistent with the sheet being stretched by

the moving substrate. Inspection of the dimensionless relation, Eq. (13a), and with the expression for α in Eq. (6b), indicates that σ_e decreases as arc length increases with other parameter values fixed. This is accomplished, according to Figs. 3–6, by reducing the value of the curvature, κ, which corresponds to a smaller pressure drop across the extruded sheet according to Eq. (7). Inspection of the dimensional functionality, Eq. (13b), indicates that this dimensionless trend does correspond to a dimensional physical trend where the pressure drop across an extruded sheet is adjusted for fixed-fluid type, geometry, and intersection angle. So, it is deduced that relatively large dimensional tensions are inherent in extruded sheets of small length, and these are incurred for large values of the imposed pressure drop.

A comparison between the expressions for the coating window, Eq. (12), and tension, Eq. (13b), reveal similar dimensional dependences (these are in parentheses in each expression). These expressions indicate that the size of the dimensional pressure windows, shown in dimensionless form in Figs. 12–14, increases for larger values of the characteristic viscosity, η^*, for larger values of the volumetric flow, Q, and for smaller values of the die to substrate spacing, L. This expansion in the dimensional windows, in general, corresponds to overall increases in tension in the extruded sheet. As is intuitive, higher tension sheets can support larger pressure drops; this, in turn, increases the size of the coating window.

We now comment on the approximate nature of the boundary conditions applied at the die slot ($s = 0$) and substrate ($s=s_L$). The analysis of entrance and end effects neglected in this analysis actually determines the correct boundary conditions to be applied. Unfortunately, the equations governing the mathematics in these regions are more complex than those given by Eq. (2) because the approximation of a gradually thinning extruded sheet does not apply (flow variations in the direction of flow and across it are of the same order). Boundary conditions valid for the simplified governing equations are obtained by using the physical features of the local regions at their outer extremities where the governing Eqs. (2) become valid. Entrance effects, such as die swell, could thus be incorporated into the extruded sheet analysis by reinterpreting the slot height, D, as the local thickness of the extruded sheet at a small distance downstream from the slot itself. If the length of the region of die swell is small compared with the overall length of the extruded sheet, this die swell can be imposed directly at the slot itself as an adjusted value of D (even if the actual slot height is different).

At the bottom of the extruded sheet, the angle and speed constraints could be determined by local analysis and imposed similarly to constraints at the slot. Note that one severe restriction on the analysis presented here is that the angle θ_L is a free parameter. Nevertheless, physical reasoning suggests that this angle is relatively small, since the substrate pulls the extruded sheet forward, and so this uncertainty is somewhat mitigated. This is reinforced by results of Figs. 13 and 14, which show that the size of the coating window does not change very much for small θ_L. This is despite the fact that variations in the angle θ_L, even when small, can have a large effect on the shape of extruded liquid sheets for small curvatures (cf. Figs. 3 and 5). At small curvatures, the pressure drop incurred is small and does not largely affect the location of the lower bound on the pressure window. The upper bound on the pressure window, however, involves sheets having shapes with similar arc lengths for small θ_L. The net effect of these two trends is a relative insensitivity in coating window to angle when it is small.

Despite the uncertainty in boundary conditions, operation limits on the extrusion coating process can be elucidated with the solution to Eq. (2) since the *form* of the applied boundary conditions are not to be expected to change even with improved accuracy in their numerical values. Uncertainties in these constraints translate to an increased margin of error in model predictions compared with experiment, and the size of the operating parameter space must be reduced to be conservative enough to compensate. When experiments are performed, a semi-empirical adjustment of the boundary conditions in the model is likely required to achieve a more quantitative result. The need for empirical adjustment is further emphasized by the fact that satisfaction of Eq. (10) is only a *necessary* condition for extrusion coating. In practice, it is not a sufficient condition because other failure modes, such as air entrainment, will further limit the operating space. Even within this more restrictive operating space, the ability to resist perturbations to disturbances will generally make one operating condition more desirable than another. The issue of disturbances cannot be directly assessed with the current steady analysis, but it requires a frequency response examination of the governing time-dependent equations. Nevertheless, we note that Figs. 3–6 reveal that arc lengths for sheets having small curvatures are especially sensitive to variations in curvature. According to the above discussion, this suggests that there is likely a large sensitivity of the extruded liquid sheet, and subsequent coating quality on the substrate, to ambient pressure fluctuations when the pressure drop across the sheet, is small.

5. Summary

It has been demonstrated that the physics of a two-dimensional gradually thinning viscous liquid sheet is critical in determining the extrusion coating window. The shape and flow field within this sheet have been derived analytically for power law liquids. The centerline shape of the liquid sheet is circular when a pressure drop is applied, despite the fact that surface tension forces, which typically give rise to circular shapes in narrow gaps, are neglected. The stretching of the viscous-dominated liquid sheet, however, gives rise to an effective tension that plays an analogous role to surface tension. The range of allowable applied pressures in extrusion coating, which defines the coating window in this work, is deduced via geometrical

considerations of a circular shape, constrained in the narrow gap; extrusion coating fails when a liquid sheet cannot be constructed successfully. Practically, the coating window defined in this paper provides necessary, but not sufficient, conditions to achieve successful coating. As discussed, uncertainty in the applied boundary conditions, as well as other phenomena not accessible via the analysis provided here, will further limit the predicted operating range of an extrusion coating process.

Notation

Ca	capillary number
d	final liquid film thickness coated on substrate
D	slot height
g	gravitational constant
G	gravitational dimensionless group
h	dimensionless local thickness of extruded liquid sheet
H	local thickness of extruded liquid sheet
L	gap spacing between slot and substrate
n	power-law exponent
m	consistency coefficient in power-law exponent
p_{down}	dimensionless ambient air pressure applied on downstream interface
P_{down}	ambient air pressure applied on downstream interface
p_{up}	dimensionless ambient air pressure applied on upstream interface
P_{up}	ambient air pressure applied on upstream interface
Q	volumetric flow rate per unit width
Re	Reynolds number
s	dimensionless arc length coordinate measuring distance along sheet centerline
S	arc length coordinate measuring distance along sheet centerline
S_L	arc length of sheet centerline
u	dimensionless local speed of liquid in sheet
U	local speed of liquid in sheet
v_s	dimensionless substrate speed; equivalent to thickness ratio D/d
V_s	substrate speed
x	dimensionless Cartesian coordinate measuring vertical distance from slot to substrate
X	Cartesian coordinate measuring vertical distance from slot to substrate
x_c	x coordinate of the extruded sheet's centerline (dimensionless)
y	Cartesian coordinate measuring horizontal distance parallel to substrate
y_c	y coordinate of the extruded sheet's centerline (dimensionless)
Y	Cartesian coordinate measuring horizontal distance parallel to substrate

Greek letters

α	dimensionless parameter defined in Eq. (6c)
δ	dimensionless ratio ($\equiv D/L$)
$\Delta P_{\max}$	maximum possible pressure drop across extruded sheet, given in Eq. (10)
$\Delta P_{\min}$	minimum possible pressure drop across extruded sheet, given in Eq. (10)
ϕ	local angle between tangent to centerline and vertical
ϕ_0	local angle between tangent to centerline and vertical at the slot exit ($s = 0$)
$\boldsymbol{\gamma}$	rate of strain tensor
η	generally shear-dependent viscosity
η^*	viscosity scale
κ	dimensionless curvature of sheet centerline
κ_1	minimum possible dimensionless curvature of sheet centerline
κ_2	maximum possible dimensionless curvature of sheet centerline
θ_L	angle of intersection between the sheet centerline and substrate at $S = S_L$
ρ	liquid density
σ	surface tension
σ_e	effective tensile force per unit width in liquid sheet
$\boldsymbol{\tau}$	stress tensor

Appendix A. General governing equations for the shape of a gradually thinning liquid sheet

In this appendix, the steady-state force and mass conservation equations governing a two- dimensional, gradually thinning liquid sheet are derived via a macroscopic balance. To this end, consider the sheet geometry and coordinate system shown in Fig. 2. All notation and assumptions used are as provided in the problem statement of Section 2.1. As indicated in Fig. 2, the control volume used to perform the force balance cuts through the interfaces on both sides and extends into the air over an infinitesimal distance. Note that for a gradually thinning sheet, the variation in thickness $H(S)$ is small enough on the scale of the control volume that tangent and normal vectors at both interfaces (i.e., at $N = \pm H(S)/2$) can be approximated as those along the sheet centerline.

The mass balance on the control volume is given by the simple expression:

$$\frac{\partial(UH)}{\partial S} = 0. \tag{A.1}$$

Furthermore, taking into account momentum, pressure viscous stress, gravitational, and surface tension forces on the

control volume, the following balance arises:

$$\frac{\mathrm{d}}{\mathrm{d}S}(\rho U^2 H\hat{\boldsymbol{S}}) = (P_{\mathrm{up}} - P_{\mathrm{down}})\hat{\boldsymbol{N}} + \frac{\mathrm{d}}{\mathrm{d}S}(\hat{\boldsymbol{S}}\cdot\boldsymbol{\tau}H) + \rho g H\hat{\boldsymbol{X}} + 2\sigma\frac{\mathrm{d}\hat{\boldsymbol{S}}}{\mathrm{d}S}, \tag{A.2}$$

where $\hat{\boldsymbol{S}}$, $\hat{\boldsymbol{N}}$, $\hat{\boldsymbol{X}}$, and $\hat{\boldsymbol{Y}}$ (used below) are unit vectors in the directions of their respective coordinates. An expression for the constitutive equation for the viscous stress for a power-law liquid $\hat{\boldsymbol{S}}\cdot\boldsymbol{\tau}$ in Eq. (A.2) is required. Following Taylor's derivation in Brown (1961) for a vertical sheet, and anticipating that this is valid for a gradually thinning sheet in the deflected coordinate system of Fig. 2, we assume that the rate of strain tensor, $\boldsymbol{\gamma}$, and stress tensor, $\boldsymbol{\tau}$, in the sheet satisfy:

$$\boldsymbol{\gamma} = 4\frac{\mathrm{d}U}{\mathrm{d}S}\hat{\boldsymbol{S}}\hat{\boldsymbol{S}}, \quad \boldsymbol{\tau} = 4\eta\frac{\mathrm{d}U}{\mathrm{d}S}\hat{\boldsymbol{S}}\hat{\boldsymbol{S}}. \tag{A.3a}$$

Thus, for a power-law liquid,

$$\eta = m\left|4\frac{\mathrm{d}U}{\mathrm{d}S}\right|^{n-1}, \quad \hat{\boldsymbol{S}}\cdot\boldsymbol{\tau} = m\left|4\frac{\mathrm{d}U}{\mathrm{d}S}\right|^{n-1}\left(4\frac{\mathrm{d}U}{\mathrm{d}S}\right)\hat{\boldsymbol{S}}, \tag{A.3b}$$

where the vertical lines denote absolute value.

According to the geometry of Fig. 2, the following relations between the unit vectors are obtained:

$$\hat{\boldsymbol{S}} = \hat{\boldsymbol{X}}\cos\phi + \hat{\boldsymbol{Y}}\sin\phi, \tag{A.4a}$$

$$\hat{\boldsymbol{N}} = -\hat{\boldsymbol{X}}\sin\phi + \hat{\boldsymbol{Y}}\cos\phi \tag{A.4b}$$

and, therefore

$$\frac{\mathrm{d}\hat{\boldsymbol{S}}}{\mathrm{d}S} = \hat{\boldsymbol{N}}\frac{\mathrm{d}\phi}{\mathrm{d}S}, \tag{A.4c}$$

The relations of Eq. (A.4) coupled with the constitutive Eq. (A.3) allow for a separation of Eq. (A.2) into tangential and normal components. After simplification of the left-hand side of Eq. (A.2) using the mass conservation expression Eq. (A.1), the tangential and normal components become

$$\hat{\boldsymbol{S}}: \rho H U\frac{\mathrm{d}U}{\mathrm{d}S} = m\frac{\mathrm{d}}{\mathrm{d}S}\left(H\left|4\frac{\mathrm{d}U}{\mathrm{d}S}\right|^{n-1}\left(4\frac{\mathrm{d}U}{\mathrm{d}S}\right)\right) + \rho g H\cos\phi, \tag{A.5a}$$

$$\hat{\boldsymbol{N}}: \rho H U^2\frac{\mathrm{d}\phi}{\mathrm{d}S} = P_{\mathrm{up}} - P_{\mathrm{down}} + m\left|4\frac{\mathrm{d}U}{\mathrm{d}S}\right|^{n-1}\left(4\frac{\mathrm{d}U}{\mathrm{d}S}\right)H\frac{\mathrm{d}\phi}{\mathrm{d}S} - \rho g H\sin\phi + 2\sigma\frac{\mathrm{d}\phi}{\mathrm{d}S}. \tag{A.5b}$$

Eqs. (A.1) and (A.5) are the desired governing equations for the shape of a planar liquid sheet.

In this paper, we restrict attention to the case of a thinning liquid sheet for which $\mathrm{d}U/\mathrm{d}S > 0$. Using this assumption, and making the force balance Eq. (A.5) dimensionless using the scales for the extruded sheet given by Eq. (2a) the result is

$$\hat{\boldsymbol{S}}: Re\, hu\frac{\mathrm{d}u}{\mathrm{d}s} = \frac{\mathrm{d}}{\mathrm{d}s}\left(H\left[4\frac{\mathrm{d}u}{\mathrm{d}s}\right]^n\right) + Gh\cos\phi, \tag{A.6a}$$

$$\hat{\boldsymbol{N}}: Re\, hu^2\frac{\mathrm{d}\phi}{\mathrm{d}s} = p_{\mathrm{up}} - p_{\mathrm{down}} + \left(4\frac{\mathrm{d}u}{\mathrm{d}s}\right)^n h\frac{\mathrm{d}\phi}{\mathrm{d}s} - Gh\sin\phi + \frac{2}{Ca}\frac{\mathrm{d}\phi}{\mathrm{d}s}, \tag{A.6b}$$

where the dimensionless groups Re, G, and Ca are defined in Eq. (2b). The general Eqs. (A.6) are the starting point for the analysis of a liquid sheet provided in Section 2.1.

At this point, we note that Eqs. (A.1) and (A.5) are consistent with various limiting cases in the literature. When inertial, gravitational, and surface tension terms are neglected in Eq. (A.5), and for a Newtonian liquid of viscosity μ (i.e., $n=1$, $m=\mu$), the derived equations are identical to those of Van De Fliert et al. (1995) obtained via asymptotic methods for a small aspect ratio liquid sheet (it is long and thin). In cases where viscous effects are neglected ($m=0$), Eqs. (A.1) and (A.5) reduce to the large-deflection equations derived by Finnicum et al. (1993), which in turn are shown to be asymptotically correct in the limit of small sheet aspect ratio and small deflections by Weinstein et al. (1997). Finally, for a steady and vertical planar sheet, the centerline is located along $\phi=0$ and $s=x$ in Eq. (A.5); Eqs. (A.1) and (A.5) reduce to those derived by Taylor in the appendix of the paper by Brown (1961). Again, these equations are demonstrated to be asymptotically correct for a planar liquid sheet of a small aspect ratio (Clarke, 1968; Ramos, 1996). Thus, the derived governing equations have general applicability to a variety of steady liquid sheet problems.

Appendix B. Viscosities in the extruded sheet

The viscosity variation and average viscosity in the extruded liquid sheet are calculated in this appendix. The average dimensional viscosity in the extruded sheet, $\langle\eta\rangle$ is expressed according to the following dimensionless relation:

$$\frac{\langle\eta\rangle}{\eta^*} = \frac{1}{s_L}\int_0^{s_L}\frac{\eta}{\eta^*}\,\mathrm{d}s, \tag{B.1}$$

where dimensional η is given by Eq. (A.3b) and the scaling factor η^* is given by Eq. (2c). Using the definitions in Eqs. (A.3b) and (2c), and differentiating the velocity field, Eq. (6a), the result is

$$\frac{\eta}{\eta^*} = 4^{n-1}\alpha^{(n-1)/n}\left(1 + \frac{(n-1)}{n}\alpha^{1/n}s\right). \tag{B.2}$$

The result, Eq. (B.2), indicates that *the viscosity varies linearly with arc length for* $n \neq 1$, and yields $\eta/\eta^* = 1$ when $n = 1$. Upon substitution of Eq. (B.2) into Eq. (B.1) and integrating, the final result for the average viscosity of the

extruded sheet is obtained:

$$\frac{\langle \eta \rangle}{\eta^*} = 4^{n-1}\alpha^{(n-1)/n}\left(1 + \frac{(n-1)}{2n}\alpha^{1/n}s_L\right). \quad \text{(B.3)}$$

References

Anturkar, N.R., Co, A., 1988. Draw resonance in film casting of viscoelastic fluids: a linear stability analysis. Journal of Non-Newtonian Fluid Mechanics 28, 287–307.

Aird, G.R., Yeow, Y.L., 1983. Stability of film casting of power law liquids. Industrial and Engineering Chemistry Research Fundamentals 22, 7–10.

Brown, D.R., 1961. A study of the behaviour of a thin sheet of moving liquid. Journal of Fluid Mechanics 10, 297–305.

Canning, K., Co, A., 2000. Edge effects in film casting of molten polymers. Journal of Plastic Film & Sheeting 16, 188–203.

Carvalho, M.S., Kheshgi, H.S., 2000. Low-flow limit in slot coating: theory and experiments. A.I.Ch.E. Journal 46 (10), 1907–1917.

Clarke, A., Weinstein, S.J., Moon, A.G., Simister, E.A., 1997. Time-dependent equation governing the shape of a two-dimensional liquid curtain, Part II: Experiment. Physics of Fluids 9 (12), 3637–3644.

Clarke, N.S., 1968. Two-dimensional flow under gravity in a jet of viscous liquid. Journal of Fluid Mechanics 31, 481–500.

D'Halewyu, S., Aggasant, J.F., Demay, Y., 1990. Numerical simulation of the cast film process. Polymer Engineering and Science 30 (6), 335–340.

Ding, F., Giacomin, J.A., Slattery, J.C., 2000. Angular plane curtain coating by drawdown of extruded polymer. Journal of Coatings Technology 72 (900), 63–68.

Ding, F., Giacomin, J.A., Slattery, J.C., 2001. Sheet coating by drawdown of extruded polymer. Journal of Coatings Technology 73 (921), 127–134.

Dobroth, T., Erwin, L., 1986. Causes of edge beads in cast films. Polymer Engineering and Science 26 (7), 462–467.

Finnicum, D.S., Weinstein, S.J., Ruschak, K.J., 1993. The effect of applied pressure on the shape of a two-dimensional liquid curtain falling under the influence of gravity. Journal of Fluid Mechanics 255, 647–665.

Hens, J., Boiy, L., 1986. Operation of the bead of a pre-metered coating device. Chemical Engineering Science 41, 1827–1831.

Higgins, B.G., Scriven, L.E., 1980. Capillary pressure and viscous pressure drop set bounds on coating bead operability. Chemical Engineering Science 35, 673–682.

Iyengar, V.R., Co, A., 1993. Film casting of a modified Giesekus fluid: a steady-state analysis. Journal of Non-Newtonian Fluid Mechanics 48, 1–20.

Kheshgi, H.S., 1989. Profile equations for film flows at moderate Reynolds numbers. A.I.Ch.E. Journal 35 (10), 1719–1727.

Kheshgi, H.S., Kistler, S.F., Scriven, L.E., 1992. Rising and falling film flows: viewed from a first-order approximation. Chemical Engineering Science 47, 683–694.

Kistler, S.F., Schweizer, P.M., 1997. Liquid Film Coating. Chapman Hall, London.

Levich, V.G., 1962. Physiochemical Hydrodynamics. Prentice-Hall Inc., Englewood Cliffs, NJ.

Matovich, M.A., Pearson, J.R., 1969. Spinning a molten threadline. Industrial and Engineering Chemistry Research Fundamentals 8 (3), 512–520.

Ramos, J.I., 1996. Planar liquid sheets at low Reynolds number. International Journal for Numerical Methods in Fluids 22, 961–978.

Ruschak, K.J., 1976. Limiting flow in a pre-metered coating device. Chemical Engineering Science 31, 1057–1060.

Saito, H., Scriven, L.E., 1981. Study of coating flow by the finite element method. Journal of Computational Physics 42, 53–76.

Sakaki, K., Katsumot, R., Kajiwara, T., Kazumori, F., 1996. Three-dimensional flow simulation of a film-casting process. Polymer Engineering Science 36 (13), 1821–1831.

Sartor, L., 1990. Slot coating: fluid dynamics and die design. Ph.D. Thesis, University of Minnesota.

Satoh, N., 2001. Viscoelastic simulation of film casting process for a polymer melt. Polymer Engineering Science 41 (9), 1564–1579.

Silgay, D., Demay, Y., Agassant, J.F., 1998. Stationary and stability analysis of the film casting process. Journal of Non-Newtonian Fluid Mechanics 79, 563–583.

Van De Fliert, B.W., Howell, P.D., Ockenden, J.R., 1995. Pressure-driven flow of a thin viscous sheet. Journal of Fluid Mechanics 292, 359–376.

Weinstein, S.J., Clarke, A., Moon, A., Simister, E.A., 1997. Time-dependent equations governing the shape of a two-dimensional liquid curtain, Part 1: Theory. Physics of Fluids 9 (12), 3625–3636.

Weinstein, S.J., Ruschak, K.J., 2004. Coating flows. Annual Review of Fluid Mechanics 36, 29–53.

Yeow, Y.L., 1974. On the stability of extending films: a model for the film casting process. Journal of Fluid Mechanics 66, 613–622.